VENTILATION AND DEDUSTING OF MELTING SHOPS

Robert KICKINGER[1], Philipp GITTLER[1], Mirko JAVUREK[1] and Johann LEHNER[2]

[1] Johannes Kepler University, Fluidmechanics Department, Altenbergerstr. 69, 4040 Linz, AUSTRIA

[2] VOEST-ALPINE Industrieanlagenbau GmbH, Turmstr. 44, 4031 Linz, AUSTRIA

ABSTRACT

CFD simulations of ventilation and dedusting systems in melting shops with an electric arc furnace are presented. The models include free and forced convection, multiphase flow and complex geometry. Special emphasize is given to the modelling of the dust phase: An Euler-Lagrangian discrete random walk approach, the stochastic transport of particles (STP) model and an algebraic drift flux model are briefly reviewed and applied in simulation. While application of the STP-model was unsuccessful, both the Euler-Lagrange approach and the drift flux model perform well, with the drift flux model being more computationally efficient. Studies on the influence of blower (ID fan) power and the effect of turbulence modelling (standard and RNG k-ε model) on dust dispersion are included. The numerical studies resulted in the optimization of blower power together with the crane/trolley arrangement and the canopy hood design.

NOMENCLATURE

c_p specific heat capacity
D_p particle diameter
Gr Grashof number
k turbulent kinetic energy
m_D total mass of dust particles in plant
m_P mass of dust particle
p pressure
Re Reynolds number
T temperature
t time
u velocity
u_P particle velocity
x_j jth coordinate direction in space
α volume fraction of dust
β thermal expansion coefficient
ε turbulent dissipation rate
λ thermal conductivity
μ dynamic viscosity
ρ density of air
ρ_P density of dust particles

INTRODUCTION

In electro steel making processes a large amount of dust is created: During charging off-gases are generated directly above the electric arc furnace (EAF) due to the burning of oil containing scrap. During melting the off-gases are emitted into the plant by the EAF through openings for the electric power supply and the oxygen lance. Usually a dedusting system consists of two parts: the primary off-gas suction system attached to the EAF via the elbow duct and the secondary offgas suction fitted on the roof of the melting shop (see Fig. 1 and Fig. 2) above the EAF. These suction systems must be designed properly in order to achieve a minimum dust concentration at working areas at a given suction mass flow or vice versa. As typical power consumptions for the suction system are in the range of 1 - 2 MW there is a great potential for savings. This paper deals with the simulation and design of secondary dedusting systems by means of CFD. Basic ideas have been considered by Birat (1997) and a similar system was studied by Ishii et al. (1997).
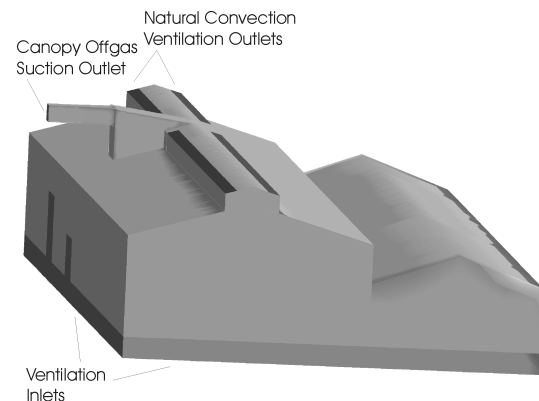
Figure 1: Industrial plant with various ventilation inlets and outlets.

GEOMETRY AND GRID

A very detailed modelling of a melting-shop is not practicable due to the complex geometry. The question which components of an industrial plant have a large impact on the flow pattern cannot be answered easily. For this study we included the following components into our CFD model:

- boundaries of the plant (floor, sidewalls, roof)
- canopy hood and partition side walls
- electric arc furnace
- off-gas suction
- ventilation inlets and outlets
- platforms and large transformers
- crane, trolley and scrap basket (for the simulation of the charging process)

Some of these are displayed in Fig. 1 and Fig. 2. The benefits of unstructured meshing techniques and adaptive grid refinement have been consequently used to create a computational grid which is dense in relevant regions and coarse elsewhere.
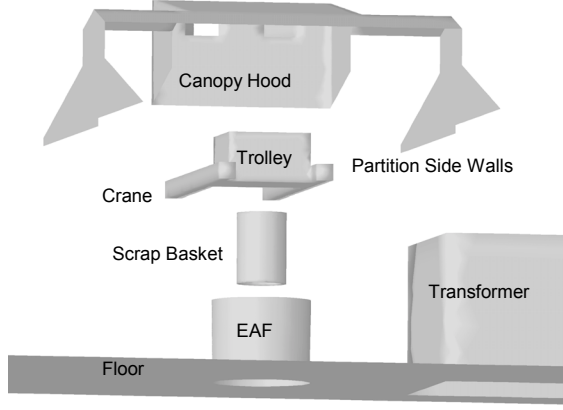
Figure 2: Configuration 2 (Trolley mounted between craneways).

MATHEMATICAL MODELLING

The Rayleigh number

$$Ra = \frac{g\beta\Delta T H^3 \rho^2 c_P}{\mu\lambda} \sim 4.5 \cdot 10^{14} \qquad (1)$$

where $H = 30$ m is the typical height of the building, indicates a highly turbulent plume, hence a turbulent formulation was followed:

Governing Equations

The Reynolds-averaged mass, momentum and energy equations are considered. This set of conservation equations is well known and not given here.

Turbulence Modelling

To close the above equations the standard k-ε model (Launder and Spalding, 1972) and the RNG k-ε model (Yakhot and Orszag, 1992) have been used. The RNG model extends the standard k-ε model by an analytically derived differential formula for the effective viscosity accounting for low-Reynolds-number effects and other features such as an additional term in the transport equation for ε.

Modelling Natural Convection

The ratio of buoyancy and inertial forces

$$\frac{Gr}{Re^2} = \frac{\Delta\rho g H}{\rho u^2} \sim \frac{0.6 \cdot 10 \cdot 30}{1 \cdot 6^2} = 5 \qquad (2)$$

where $u = 6$ m/s is a typical velocity in the plume, indicates strong buoyancy contributions to the flow. To account for natural convection the Boussinesq approximation and the ideal gas law have been used in simulations.

Boundary Conditions

Standard wall functions (Launder and Spalding, 1974) have been used and all walls have been considered smooth. Ventilation inlets and outlets have been modelled as pressure boundary conditions. The off-gas suction outlet was modelled as velocity boundary condition. Typical values in the secondary off-gas duct range from 8 to 25 m/s.

Electric Arc Furnace

The furnace is emitting energy and hot gases as well as dust into the plant. In simulations the mass flow and temperature of emission gases have been prescribed. These parameters have been computed by an EAF simulation tool developed by VAI and described in Hofer et al. (1997). In the CFD simulations radiation was neglected in general.

Diffusion/Convection Transport Model

We consider a Species Transport Model without chemical reactions and laminar mass diffusion, given by

$$\frac{\partial}{\partial t}(\rho m'_i) + \frac{\partial}{\partial x_j}(\rho u_j m'_i) = \frac{\partial}{\partial x_j}(\frac{\mu_t}{Sc_t}\frac{\partial m'_i}{\partial x_j}). \quad (3)$$

Here m'_i is the mass fraction of species i, μ_t is the turbulent viscosity and the turbulent Schmidt number is set to

$$Sc_t = 0.7 \qquad (4)$$

This model is used in the simulation of the charging process to judge how efficient a configuration sucks off dust loaden air. Of course this model is not capable of representing sedimentation and simulations apply to the dust particles, that move with the flow of the continous phase.

Euler-Lagrangian Discrete Random Walk Model

In this model the trajectory s of a dust particle is computed by integrating the force balance

$$m_P \frac{du_P}{dt} = F_D + F_g + F_m + F_p \qquad (5)$$

in a Lagrangian reference frame. Here

$$F_D = m_P \frac{18\mu}{\rho_P D_P^2} \frac{C_D Re_P}{24}(u - u_P) \qquad (6)$$

denotes the drag force and

$$Re_P = \frac{\rho D_P |u - u_P|}{\mu} \qquad (7)$$

is the relative Reynolds number. C_D is the drag coefficient for smooth spherical particles following Morsi and Alexander (1972). The term

$$F_g = m_P g_s (1 - \frac{\rho}{\rho_P}), \qquad (8)$$

where g_s is the projection of the gravitation vector on the coordinate along particle trajectory, regards to gravitation and accounts for sedimentation effects.

$$F_m = \frac{1}{2} m_P \frac{\rho}{\rho_P} \frac{d}{dt}(u - u_P) \qquad (9)$$

is the force necessary to accelerate the surrounding fluid (added mass concept). Because of the large difference in density

$$\frac{\rho_P}{\rho} \sim 3000 \qquad (10)$$

the influence of the added mass force is small, however it is included in the simulations.

$$F_p = m_P \frac{\rho}{\rho_P} u_P \frac{dp}{ds} \qquad (11)$$

is the force acting due to pressure gradients in the fluid. Turbulent dispersion is modelled by a discrete random walk method (stochastic tracking technique), see Fluent

Inc. (1998). The effect of the dispersed phase on the continous phase is realised by source terms in the continous phase equations. The continous and dispersed phase equations are solved alternately until the solutions in both phases have converged. The modelled particle size distribution is given in Table 1, where γ indicates the mass fraction for each particle diameter. This discrete spectrum is representative for a measured continous spectrum.

D_p [μm]	γ [%]	u_D [m/s]
100	15	$6.5 \cdot 10^{-1}$
10	70	$9.1 \cdot 10^{-3}$
1	10	$9.1 \cdot 10^{-4}$
0.1	5	$9.1 \cdot 10^{-7}$

Table 1: Particle size distribution and drift velocities.

Stochastic Transport of Particles Model

While the Discrete Random Walk method is based on the averaging of a large number of random particle trajectories the stochastic transport of particles (STP) model follows a rigorous mathematical approach. Turbulent dispersion of particles in gas flows about a mean trajectory is calculated using statistical methods: The concentration of particles about a mean trajectory is represented by a multivariante Gaussian probability function (PDF)

$$P(x_i,t) = \frac{e^{-s/2}}{(8\pi)^{3/2} \prod_{i=1}^{3} \sigma_i}, \quad (12)$$

where

$$s = \sum_{i=1}^{3} \left(\frac{x_i - \mu_i}{\sigma_i} \right)^2. \quad (13)$$

The geometrical position $\mu_i(t)$ represents the most likely position of a particle (the center of the particle cloud). The variances σ_i^2 of the PDF are based on the degree of particle dispersion due to turbulent fluctuations and they can be expressed as a function of the mean square velocity fluctuations and the particle velocity correlation function (Baxter and Smith, 1993). Therefore the modelling of the particle velocity correlation function determines the particle dispersion (Wang, 1990). The mean trajectory is obtained by solving the ensemble-averaged equations for all particles represented by the PDF.

Algebraic Drift Flux Model

This multiphase flow model for interpenetrating media in general solves the continuity and momentum equation for the mixture and a volume fraction equation for each additional phase. It allows the phases to move at different velocities and the drift velocity of phase j

$$\vec{u}_{D,j} = \vec{u}_j - \vec{u}_m, \quad (14)$$

where u_m is the mixture velocity, is given by an algebraic expression. Since the maximum mass fraction of dust is very low in this application,

$$\alpha \frac{\rho_P}{\rho_m} < 0.003, \quad (15)$$

the contribution of the dust phase to the mixture density and mixture velocity can be neglected:

$$\rho_m = \rho$$
$$u_m = u \quad (16)$$

Therefore the drift velocity of the primary phase vanishes

$$\vec{u}_{D,air} = \vec{0} \quad (17)$$

and the drift velocity of the dust phase is computed by an analysis of Eq. 5: We consider an unaccelerated motion (local equilibrium between the phases) and neglect the influence of pressure gradients (due to Eq. 10) and obtain

$$\vec{u}_D = \frac{24 \rho_P D_P^2}{18 \mu C_D \, \mathrm{Re}_P} \vec{g}. \quad (18)$$

for the drift velocity of the dust particles. With the drag coefficient C_D as given by Morsi and Alexander (1972) Eq. 18 is a quadratic equation for the drift velocity and numerical values for different particle diameters are given in Table 1. The assumption of local equilibrium can be justified by the fact, that particle acceleration occurs only in short time scales (and therefore in short spatial length scales) before gravitation and drag forces equal each other. With the influence of turbulent diffusion the volume fraction equation for the dust phase reads

$$\frac{\partial}{\partial t}(\alpha\rho) + \frac{\partial}{\partial x_i}(\alpha\rho u_i) =$$
$$= \frac{\partial}{\partial x_i}(\frac{\mu_t}{Sc_t} \frac{\partial}{\partial x_i}(\frac{\alpha\rho_P}{\rho}) - \alpha\rho u_{Di}) \quad (19)$$

As a consequence of Eq. 16 the volume fraction equation is decoupled from the other field equations (for the mixture), which are (again due to Eq. 16) equal to those of the gas phase. Boundary condition for the volume fraction equation are as follows: Prescribed volume fraction at inlets and zero gradient at vertical walls. Sedimentation on non-vertical walls was implemented by source terms in the neighbouring cells.

RESULTS AND DISCUSSION

All simulation results have been obtained using the commercial CFD code Fluent 5 (and the former version Fluent/UNS) extended by user defined routines. Dominated by natural convection, the flow in the ventilated plant with a heat source is quite sensitive and convergence in numerical simulation can only be reached by using an unsteady solver. This indicates that no steady solution exists for this type of flow, see also Reynolds (1998). If the plant has only a few ventilation inlets the whole flow pattern (in simulation) shows great dependance on the direction vector of the inflowing air. This parameter was determined by separate CFD simulations taking into account the complex geometry (noise reduction devices and window shades) of the ventilation inlets (Mitter, 1998). Velocity vectors during the melting process are displayed in Fig. 3.
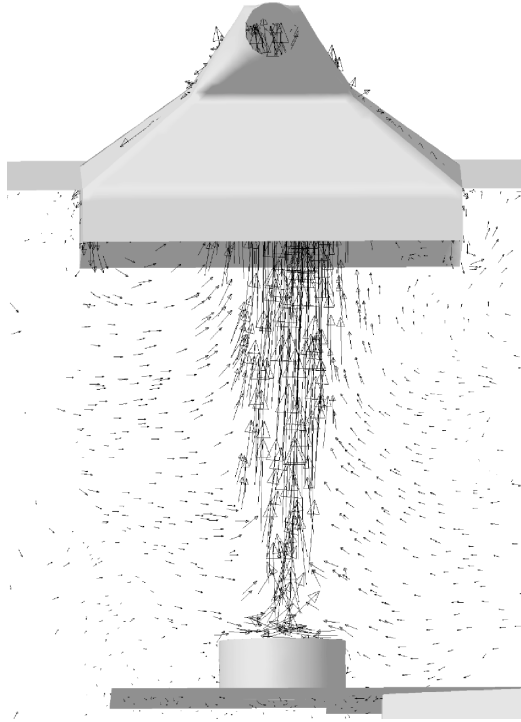
Figure 3: Plume velocity vectors during melting.

STP-Model

While this model was succesfully applied to simple flows (Baxter and Smith, 1993), its application for this particular flow proved as very difficult and suffers from a principal drawback: As most of the dust is sucked off by the ventilation and only a small percentage of the total amount of dust sediments in the plant (as a consequence of turbulent dispersion), the mean cloud trajectories leave the computational domain through the ventilation outlet and very large maximum cloud diameters are necessary to account for the effects of sedimentation. In combination with long particle residence times before sedimentation occurs this leads to excessive simulation times prohibting the successful application of this model in the present form and with the computer hardware available.

	Run 1	Run 2	Run 3	Run 4
m_D [kg]	2.46	1.81	1.99	2.93
c_D [10^{-6} kg/m³]	13.96	7.97	9.11	6.55
c_O [10^{-3} kg/m³]	0.189	0.186	0.187	0.192
dm_O [10^{-3} kg/s]	25.5	25.05	25.14	25.86

Table 2: Results from discrete random walk simulations.

Euler-Lagrangian Disrete Random Walk Model

Table 2 gives results from four runs showing the statistical nature of the discrete random walk model. In this study up to 40000 trajectories with up to 300000 steps in space per DPM-iteration have been computed. The dust concentration in the off gas c_O (and therefore the mass flow of dust in the offgas dm_O) scatter in a very narrow bandwidth while the total amount of dust in the plant m_D and the average dust concentration in working areas c_D scatter by a factor ~ 2. This indicates that the number of particles tracked and the number of steps is sufficient but accuracy could be increased by calculating more and longer particle trajectories. However the discrete random

walk approach is extremely CPU intensive as it is necessary to compute a large number of particle trajectories to get some statistical safety.
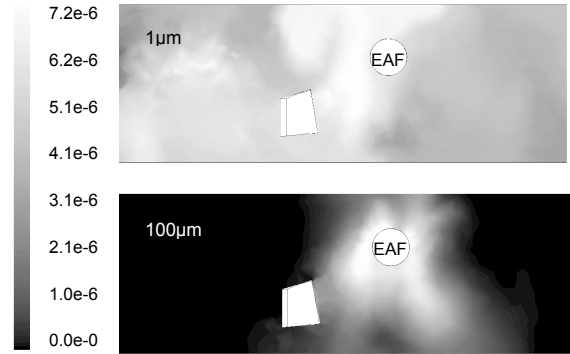
Figure 4: Contours of dust concentration [kg/m³] in head-height over platforms.
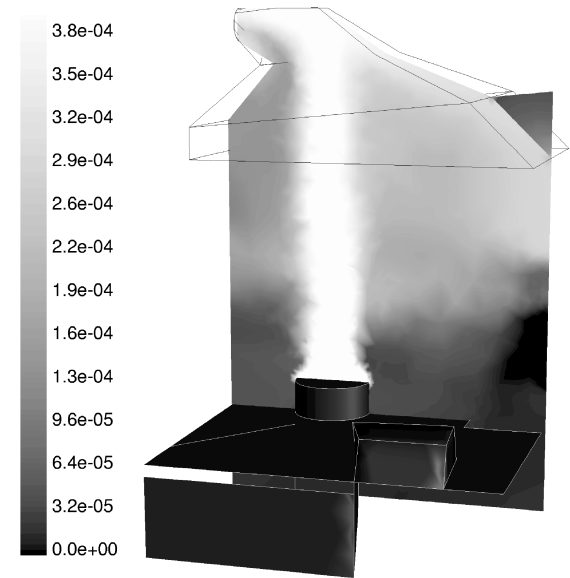
Figure 5: Contours of dust concentration [kg/m³] on a vertical plane.

Algebraic Drift Flux Model

When applying this model to secondary phases with non-uniform paricle size distribution one approach is to compute a mass weighted average drift velocity and solve one transport equation for the volume fraction. The alternative (followed in this article) is to solve an additional equation for the volume fraction of each particle size (as given in Table 1). This approach provides information about the influence of particle size on dispersion. The concentration of 1μm- and 100μm-particles is displayed in Fig. 4 clearly indicating, that 100μm-particles primarily sediment in the vicinity of the EAF, while 1μm-particles are distributed over the whole plant. The overall dust concentration (sum of all individual particle size concentrations) on a vertical plane is given in Fig. 5. The influence of clean air entering through a ventilation inlet is clearly visible. The total mass of dust in the plant m_D and the average dust concentration in working areas c_D are given in Table 3. In general the drift flux approach is robust and economic in terms of computational resources compared to the discrete random walk approach. Furthermore contrary to the Euler-

Lagrange model efficient parallelisation in the framework of a commercial CFD package is no problem.

	0.1μm	1μm	10μm	100μm	sum
m_D [kg]	0.72	1.42	8.5	0.2	10.8
c_D [10^{-3}g/m³]	2.5	5.1	33	1	41.6

Table 3: Dust phase simulation results (Drift flux model).

Discussion of Dust Phase Simulation Results

As can be seen from Tables 2 and 3 simulation results for the total mass of dust particles in the plant m_D and the average dust concentration in working area c_D obtained by the drift flux model are ~ 4 times higher than for the Euler-Lagragian discrete random walk approach. This large difference implies some questions: How can this large difference be explained? Is the drift flux model overshooting or the Euler-Lagragian approach undershooting dust concentration? Possible explanations (include among others) a too small choice of the turbulent Schmidt number Sc_t in the drift flux model resulting in too high particle dispersion. The measured value of average dust concentration in working areas $c_D = 6 \cdot 10^{-6}$ kg/m³ is very close to the Euler-Lagrangian simulation result. However this is not very useful in answering the question, which approach is closer to reality, because the dust concentration in both models basically depends on the volume fraction of dust at the EAF (the only source of dust in the model). This parameter was computed by DynEAF (Hofer et al., 1997) and is very difficult to measure and therefore has not been validated by measurements so far. However dispite the quantitative discrepancy the qualitative correlation of simulation results of both models is good and both models can be applied successfully for the comparison of configurations.
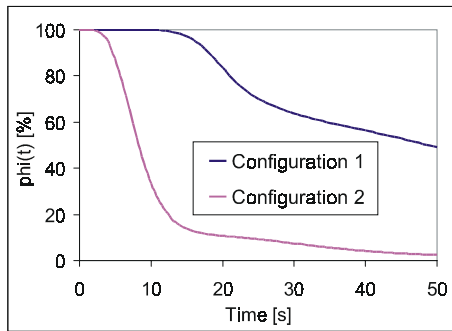
Figure 6: Mass fraction for two different configurations.

Geometrical Optimizations

When optimizing configurations, both the melting process and the charging process must be considered. Evaluation of configurations with regard to the melting process is done as detailed above with results from the drift flux model or the Euler-Lagrangian approach. To judge how efficient a configuration sucks off dust loaden air during charging the diffusion/convection transport model is used in simulations: From observations the area where dust and heat are generated during the charging process is known. The gas in this area is initialized at time $t = 0$ to consist of species 2 (dust-loaden air) exclusively,

$$m'_2 = 1 \text{ and } m'_1 = 0 \text{ at dust generation area,} \qquad (20)$$

while the gas in the complementary part of the plant is initialized to consist of species 1 (clean air)

$$m'_2 = 0 \text{ and } m'_1 = 1 \text{ elsewhere.} \qquad (21)$$

By solving the diffusion/convection transport equation Eq. 3 we obtain graphs $\varphi(t)$ as shown in Fig. 6 by integrating the mass fraction $m'_2(t)$ over the computational domain and dividing through the initial mass of species 2 at time $t = 0$

$$\varphi(t) = \frac{\int \rho m'_2(t)dV}{\int \rho m'_2(t = 0)dV}. \qquad (22)$$
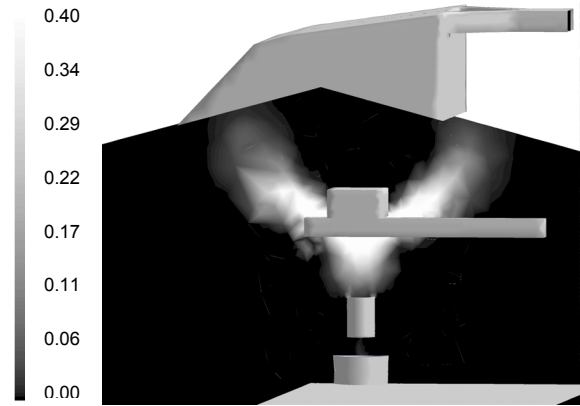
Figure 7: Contours of mass fraction of specie 2 m'_2 [1] during charging (Configuration 1).
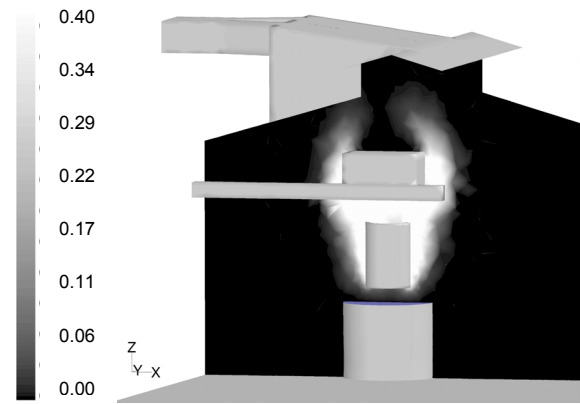
Figure 8: Contours of mass fraction of specie 2 m'_2 [1] during charging (Configuration 2).

As one major design improvement we describe the optimization of the crane/trolley arrangement: In Configuration 1 the thermal plume is split by the crane/trolley arrangement (see Fig. 7) and one part of the plume is directed towards the roof of the plant resulting in a large recirculation region above the trolley and in poor suction performance (Fig. 6). This effect is due to the unappropriate design of the crane/trolley arrangement (see Fig. 9) which forces a quasi two-dimensional flow pattern between the craneways. This effect is completely suppressed by the optimized Configuration 2 (Fig. 8). In this optimized configuration the trolley is not mounted above but between the craneways to prevent the quasi two-dimensional splitting of the plume and to ensure, that off-gases can easily flow around the whole arrangement on

all sides. In combination simulation results of both the melting process and the charging process provide good validation criteria to judge the quality of configurations and are the basis for optimizations.

Trolley mounted above craneways
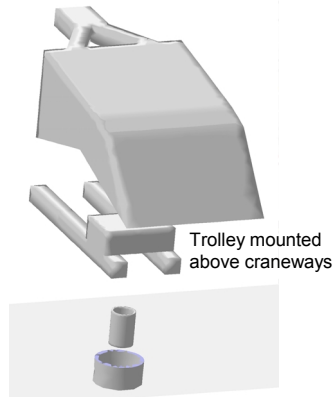
Figure 9: Configuration 1.

Comparison of Turbulence Models

As indicated in Table 4 the RNG model yields significantly smaller average values in turbulent kinetic energy k_{avg} and turbulent dissipation rate ε_{avg}, while the average velocity u_{avg} is very similar. In combination with the discrete random walk model this results in smaller turbulent particle dispersion and therefore smaller values in dust concentration. m_D denotes the total mass of dust in the plant and c_D is the average dust concentration in working areas.

	k-ε model	RNG model
u_{avg} [m/s]	0.49	0.52
k_{avg} [m²/s²]	0.76	0.22
ε_{avg} [m²/s³]	0.16	0.039
m_D [kg]	5.55	2.3
c_D [10⁻⁶ kg/m³]	16.7	9.4

Table 4: Discrete random walk model results using different turbulence models.
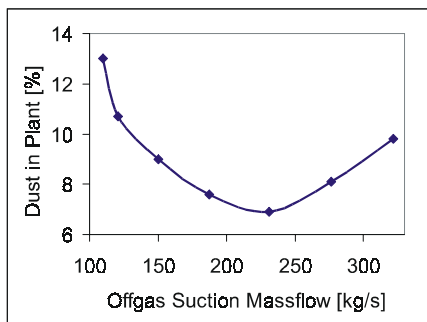
Figure 10: Dust/off-gas-suction-massflow relation for an inappropriate designed configuration.

Variation of Blower Power

It sounds trivial that increasing blower (ID fan) power (and therefore offgas suction mass flow) results in smaller values of dust concentration. But relations in fluid mechanics are mostly nonlinear and for an inappropriate configuration of ventilation inlets an increase in blower power can actually lead to higher overall dust

concentrations in the plant as shown in Fig. 10. The numerical values in Fig. 10 have been obtained using the Euler-Lagrangian discrete random walk approach and indicate the percentage of dust particles which are not sucked off and sediment in the plant. This effect can be explained by the influence of a free jet from a nearby ventilation inlet pushing the plume partly outside of the canopy hood. However this will not happen in a properly designed melting shop.

CONCLUSION

CFD is a powerful tool for the design of ventilation and dedusting systems: The simulation of existing or projected systems reveals the weaknesses of a configuration. With the detailed knowledge obtained by the simulations optimizations can be proposed and shown to be effective.

ACKNOWLEDGEMENTS

REFERENCES

BAXTER L. L. and SMITH P. J.: "Turbulent Dispersion of Particles: The STP Model", *Energy & Fuels*, 7, 852-859, 1993.

BIRAT J. P.: "Modelisation et conduite des processus sidururiques", *La Revue de Metallurgie-CIT*, Novembre 1997.

FLUENT INC.: *User's Guide for FLUENT 5*, Lebanon, NH, USA, 1998.

HOFER M., STEGER P. L., LEHNER J., GEBERT W.: "Improved EAF Design and Operation using the DynEAF Simulation Tool", *Iron & Steel Review*, Vol. 40, No. 9, 35-42, 1997.

ISHII K., KAWAKAMI H., MURAHASHI Y., TANAKA K.: "Development of New Engineering Technology Based on Computer Analysis of Dust Diffusion", *Nippon Steel Technical Report No. 74*, 1997.

LAUNDER B. E. and SPALDING D. B. *: Lectures in Mathematical Models of Turbulence*, Academic Press, London, England, 1972.

LAUNDER B. E. and SPALDING D. B.: "The Numerical Computation of Turbulent Flows", *Computer Methods in Applied Mechanics and Engineering*, 3:269-289, 1974.

MITTER R.: "Projekt Fensterdurchstroemung", *CFD-Praktikumsbericht*, Fluidmechanics Department, Johannes Kepler University Linz, Austria, 1998.

MORSI S. A. and ALEXANDER A. J.: "An Investigation of Particle Trajectories in Two-Phase Flow Systems", *J. Fluid Mechanics*, 55 (2): 193-208, 1972.

REYNOLDS A. M.: "Modelling particle dispersion within a ventilated airspace", *Fluid Dynamics Research*, 22:139-152, 1998.

YAKHOT V., ORSZAG S. A.: "Renormalization Group Analysis of Turbulence. I. Basic Theory", *J. of Scientific Computing*, Vol 1, No. 1, 1-151, 1992.

WANG L. P.: *On the Dispersion of Heavy Particles by Turbulent Motion*, PhD Thesis, Washington State University, 1990.